Performance Efficiency of Tubular Inorganic Membrane Modules for Pervaporation

Stefan Sommer and Bernd Klinkhammer
Shell Deutschland Oil GmbH, Rheinland Raffinerie, Werk Wesseling, 50389 Wesseling, Germany

Michael Schleger and Thomas Melin
Institut für Verfahrenstechnik, Rheinisch Westfaelische Technische Hochschule (RWTH) Aachen, 52056 Aachen, Germany

DOI 10.1002/aic.10289
Published online in Wiley InterScience (www.interscience.wiley.com).

Because the separation performance improves the rate of transport in inorganic high flux pervaporation membranes, resistances in the boundary layer become the performance bottleneck in the dehydration of solvents. By operating the membranes at high temperature levels, permeate water fluxes of more than 10 kg m^{-2} h^{-1} can be obtained. Therefore, the design of efficient industrial-scale modules becomes significant. In this study, a set of generic rules for the construction of technical and economically feasible modules is derived and different design versions are compared, including tubular, hollow-fiber, spiral-wound, and multichannel monolith types. In particular, the performance efficiency and applicational limitations of the isothermal module concept Pervap® SMS (Silica Membrane System) from Sulzer Chemtech are evaluated. Steam condensation or a thermal liquid ensures the constant operation temperature for any permeate loading. For assessing the module efficiency the impact of concentration and temperature polarization is modeled with empirical correlations for the mass and heat transfer on the feed side. For these high-flux membranes the overall flux reduction by polarization effects in the technical module is around 30 to 50%. At lower permeate fluxes the losses in membrane performance are more the result of mass transfer limitations, whereas at higher permeation rates heat transfer becomes more significant. The pressure drop in the porous support was calculated by Knudsen diffusion, whereas the pressure loss in the permeate channel was determined with laminar flow according to Hagen–Poiseuille. At a permeate flux of 10 kg/m^2h the friction loss in the support can reach up to 100 mbar, whereas the pressure drop in the permeate tube is negligible. © 2004 American Institute of Chemical Engineers *AIChE J,* 51: 162–177, 2005
Keywords: inorganic membranes, vapor permeation, pervaporation, module design, performance efficiency, optimization

Introduction

As membrane science develops, better membrane materials are being formulated to accomplish a wide range of separations. In some cases, the membranes are so effective that the separation is limited by the rate of transport from the bulk through the boundary layer to the active membrane layer rather than through the membrane itself. In contrast, for polymeric membranes, the heat and mass transfer do not constitute a critical parameter because of the low permeate fluxes at maximum temperatures of 100° C. Recently commercialized tubular inorganic pervaporation membranes combine exceptional

Correspondence concerning this article should be addressed to S. Sommer at Stefan.Sommer@shell.com.

permeance with good selectivity. Furthermore, these membranes can be operated at much higher temperatures, thus exponentially increasing the flux rates. Thus, the actual performance of technical membrane modules may be noticeably lower than the ideal membrane performance, which is caused by additional transport resistances on the feed and permeate side. Bottlenecks for high flux membranes may become the feed-side temperature and concentration polarization. The higher permeate flux also leads to a decline in accelerated axial temperature across the module and to friction losses of the vapor flow in the porous support and in the permeate piping.

Up to now, the incentive for optimizing mass and heat transfer has not been very compelling, and in fact module design in pervaporation has hardly been studied. The majority of publications in the literature deal with module design for organic/water separation. Hickey and Gooding[1-3] investigated the use of spiral-wound membrane modules for the pervaporative removal of volatile organic compounds (VOCs) from water. They developed mass transfer correlations to carry out an economic optimization for the separation cost of the process. The effect of concentration polarization on the separation of VOCs from water by pervaporation is described by Baker et al.[4] They observed a severe reduction in flux and selectivity resulting in some unexpected permeation properties in spiral-wound modules, such as improving performance with thicker membranes and smaller driving force. Crowder and Gooding[5] evaluated the mass transfer efficiency of a spiral-wound, transversal flow, hollow-fiber module for the deoxygenation of water. Compared to traditional module designs they found at least 20% higher mass transfer rates combined with three- to fourfold higher packing densities. A general correlation of concentration polarization with hydrodynamic and geometry parameters is proposed by Mi and Hwang[6] for hollow-fiber modules. Their theory allows a distinction between the membrane and the boundary layer contribution to separation. Cussler et al. studied the mass transfer resistances within the membrane and on the feed and permeate side in PDMS hollow-fiber modules with baffles[7] and in corrugated membranes.[8] The former compared the measured coefficients with literature data, indicating feed-side controlled mass transfer resistances at high permeabilities with small and negligible resistances within the membrane and at the permeate side, respectively. The latter deals with the validation of a modified Thiele model for the performance of corrugated flat-sheet membranes with the aim of drawing conclusions from macro to nanocorrugated systems.

Lipnizki and Field[9] used an engineering approach to develop a framework for a mass transfer performance description of hollow-fiber modules with shell-side axial feed flow. With the model, different hydrodynamic effects such as dead zones, channeling, transfer flow, and surface renewal are discussed as a function of the void fraction. Also the influence of maldistribution on mass transfer performance is reflected. Lipnizki and Field[10] also investigated the integration of vacuum and sweep gas pervaporation with hollow-fiber modules for the recovery of organic compounds from wastewater. For the model substances, phenol and pyridine, the studies revealed that a combination of sweep gas with moderate vacuum is superior. A compromise has to be accepted with respect to the flow direction. The optimum hollow-fiber configuration is a shell-side feed flow for vacuum pervaporation, whereas it is tube-side feed flow for sweep gas pervaporation. In the first case the void fraction should be selected as low as possible to reduce concentration polarization. This construction is limited by the pressure constraints of the module and the process. In the second case the void fraction should be as high as possible to reduce the permeate pressure gradient. For the application of plate-and-frame modules in the same separation Lipnizki and Field[11] developed a resistance-in-series model to derive some general guidelines for the process design. The recommendations cover all major engineering parameters such as flow pattern and regime, packing density, permeate pressure, and both inlet and outlet temperatures.

Witte et al.[12] compared different module geometries for high-flux pervaporation membranes with computational fluid dynamics (CFD) tools and concluded that tubular configurations have clear advantages over standard plate-and-frame arrangements.

In this study the performance efficiency and limitations of the isothermal module concept Pervap® SMS (Silica Membrane System) from Sulzer Chemtech in the dehydration of solvents by pervaporation have been evaluated and compared to other commercially available design versions. The simulation model used is based on empirical correlations developed by Klinkhammer et al.[13] The relevant transport resistances, such as concentration and temperature polarization, axial temperature decline, and pressure drop in the porous support and permeate channel, are discussed and generic design rules are derived. The technical feasibility of the concept will be assessed, also touching on construction aspects of the module.

Module Types and General Design Aspects

There are several, sometimes conflicting, requirements for technical pervaporation modules. First, a minimization of the transport resistances in a technical optimization has to guarantee an efficient use of the installed membrane area. This is achieved by:

- High heat and mass transfer coefficients on the feed side.
- Even flow distribution (that is, avoidance of bypassing and dead zones).
- Optimal ratio of feed flow rate to membrane area.
- Low pressure drop in the porous support and permeate channels.
- Leak-proof construction of the whole system.

Second, there are a number of manufacturing, operation, and economical demands aiming at a simple, compact, easy to manage, and low-cost module:

- High packing density (membrane area per volume unit).
- Good and universal chemical and thermal stability.
- Convenient handling with easy module installation and membrane replacement.
- Low manufacturing cost.

So far, the industrial use of pervaporation has been limited to solvent dehydration and separation of water from reaction mixtures. Around 100 commissioned pervaporation plants are in operation worldwide, most of them equipped with polymeric membranes in stainless steel plate-and-frame modules. With correct hydrodynamic design their simple construction allows an evenly distributed feed flow over the membrane with negligible polarization effects.[14,15] In combination with small permeate pressure losses a high efficiency of the installed membrane area can be achieved. Important disadvantages, mainly

related to complex handling and installation, are the low packing density, material and labor-intensive module fabrication, and high leakage rates because of the numerous gaskets required.[16]

In these applications spiral-wound and capillary membrane modules are interesting alternatives because of their lower specific cost in addition to easier installation and membrane replacement. On the other hand, the hydrodynamics on the feed side are inferior and pressure drop on the permeate side is more critical. Sufficient chemical and thermal stability for the contact with solvents at high temperatures is a serious construction problem. The selection of a suitable potting or splicing material is quite difficult and welding of the standard poly(vinyl alcohol)/polyacrylonitrile (PVA/PAN) membranes is not possible. For this reason, initially developed spiral-wound and capillary polymeric membrane modules no longer exist today.[17,18] Today, capillary modules equipped with polyimide (PI) or polyetherimide (PEI) are commercially available, which are applied particularly in the dehydration of reaction mixtures by vapor permeation.[19-21]

Because inorganic membranes for pervaporation are thus far available only in tubular form, there is little choice for the design of efficient modules. The concepts are technically based on the shell-and-tube heat-exchanger design with similar geometry. Depending on the position of the separation layer, different configurations are possible. By any means the separation layer should always face the feed side, whereas the porous support has to be turned toward the permeate side.

With the active layer inside the tube, one is concerned with lumen-side feed flow. This is the case for silica membranes from Pervatech,[22] produced as single tubes (ID: 7 mm; OD: 10 mm) and A-type zeolites from Alan Cobham.[23] The latter membrane module is supplied as multichannel tubes (OD: 20 mm) and four annuli (diameter: 6 mm). When the active layer is coated on the outer surface the feed stream is on the shell side of the tube. Depending on the process parameter and operation mode with liquid or vaporized feed, one out of two potential design options will be more favorable. The stainless steel pervaporation modules from Mitsui,[24] equipped with tubular A-type zeolite membranes (OD: 12 mm; ID: 9 mm), exhibit a forced perpendicular feed flow with baffles. The zeolite tubes are sealed with a kind of shrunk-on hose from

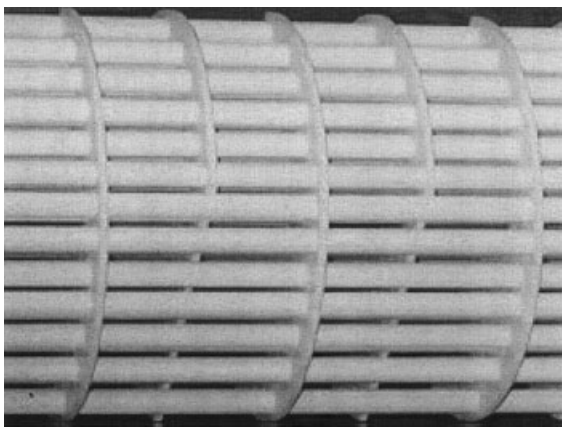

Figure 1. Shell-and-tube module with baffles and perpendicular feed flow.[24]

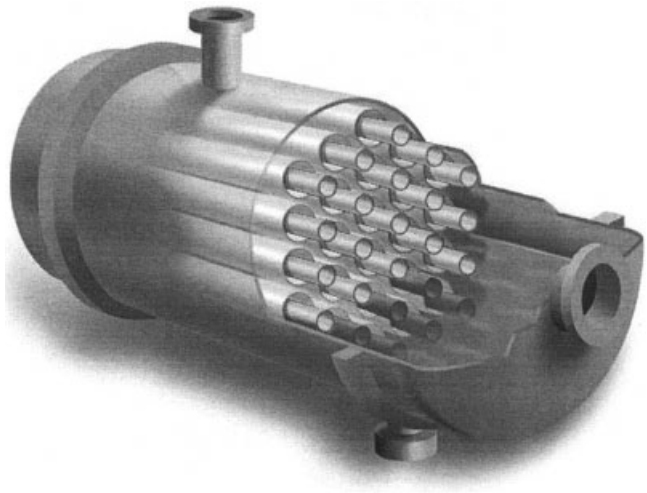

Figure 2. Design of the Pervap® SMS module with parallel feed flow in an annular duct.[14]

suitable polymers to stainless steel bolts that are assembled in a metal plate. The permeate side of the membranes is open to install the modules in vacuum vessels, the arrangement of which is shown in Figure 1.

The other option is to guide the feed parallel to the membrane in an annular duct. By installing the membranes inside the tubes of a heat exchanger, the necessary heat for evaporation of the permeate can be directly supplied in the module. This configuration has been chosen by Sulzer Chemtech[14] to commercialize amorphous silica membranes (OD: 14 mm; ID: 8 mm) under the license of ECN.[25] The design concept of the Pervap® SMS module is schematically shown in Figure 2.

The ceramic tubes are installed coaxially inside the steel tubes of a shell-and-tube heat exchanger. The tubular membranes are sealed with carbon gaskets. The feed passes through the annular gap between the tubes and the permeate is collected under vacuum from the inside of the ceramic tubes at the head flange. The membranes can be connected in parallel or in series, allowing an adjustment of the feed velocities in accordance with a certain flow rate. The pressure drop of the turnaround and in the annular duct is so small that even a complete serial connection would lead to acceptable friction losses over the whole module.[26,27] Another advantage of the turnaround is that with each passage the feed mixture is fully mixed again. Hence, even at moderate feed velocities in the annular duct, polarization effects are substantially minimized. The tube-in-tube design offers sufficient resistance to high feed pressures. The modules are available in different sizes of 1, 3, 6, and 10 m^2. The shell side can be heated by steam or thermal liquid, depending on the temperature, to ensure an isothermal operation of pervaporation. Nevertheless, all previously mentioned module types for tubular inorganic membranes have certain disadvantages.

Up to now, low packing density, special sealing of each single membrane, and complex manufacturing signify an extremely high specific module cost of around 3000 €/m^2. To overcome these general limitations of tubular geometries and to reduce production costs, capillary, spiral-wound, and monolith structures including fully ceramic modules for high-temperature applications are under development. To increase packing

density Ceramem Inc. (Waltham, MA)[28] is working on multichannel and honeycomb monolith structures. TNO (Eindhoven, The Netherlands)[29] and Fraunhofer IGB (Stuttgart, Germany)[30] have developed flexible ceramic hollow-fiber membranes that can be coated on the inside or outside. Recently, Creavis GmbH together with Degussa AG (Marl, Germany)[31] launched ceramic metal composite foils for spiral-wound modules. The HITK (Hermsdorf, Germany)[32] already presented a fully ceramic module construction. For a robust high-temperature system thermal expansion coefficients have to be taken into account. The support and housing are conjoined before the final separation layer is applied, and thus complex sealing constructions are not required.[33,34] Still a large part of the specific module cost belongs to the membrane preparation. To facilitate a cheaper production method, faster manufacturing techniques with one-step processing by microwave heating are being developed for the thermal processing of zeolite membranes.[35]

Development of Simulation Model

The simulation model and Excel-based calculation program have been developed by Klinkhammer and are described elsewhere in detail.[13] The simulation is based on an algorithm with a "succession-of-elements" method. The membrane length is divided into a large number of finite elements. Within these elements it is assumed that the driving force for mass transfer remains constant. It incorporates constant conditions for the partial pressure difference between the feed and permeate side and the physical properties of the components. The advantage of this approach is the modular implementation of parameters influencing the overall process, such as concentration and temperature boundary layer or pressure gradients on the permeate side. First, a concentration and temperature profile in the module is estimated by the inlet conditions of the feed and the resulting permeate and retentate stream for each element. The local mass and heat transport from the bulk to the membrane surface are incorporated by empirical correlations. The real profiles are determined iteratively by the calculation program using the least-square-root method. The process parameters of the final permeate and retentate stream of the pervaporation unit can thus be derived for further analysis.

Description of polarization effects on the feed side

The concentration and temperature at the membrane surface are influenced by the partial permeate flux of the components as well as by the feed-side hydrodynamics and the operation parameter. To describe the transport phenomena an engineering approach with dimensionless numbers is applied. The mass and heat transfer coefficients through the boundary layer are defined by the Sherwood (Sh) and Nusselt (Nu) numbers

$$\mathrm{Sh} = \frac{\beta d_h}{D} = f(\mathrm{Re}, \mathrm{Sc}, \text{geometry}) \tag{1}$$

$$\mathrm{Nu} = \frac{\alpha d_h}{\lambda} = f(\mathrm{Re}, \mathrm{Pr}, \text{geometry}) \tag{2}$$

By assuming a full analogy of mass and heat transfer, both numbers can be calculated with the same well-established empirical correlations for parallel flow in annular duct–type tubular membrane modules from Stephan,[36] Gnielinski,[37] and Schlünder.[38] In the following, the equations for $\mathrm{Nu} = f(\mathrm{Re}, \mathrm{Pr}, \text{geometry})$ are deduced from $\mathrm{Sh} = f(\mathrm{Re}, \mathrm{Sc}, \text{geometry})$ because of their equality.

With the hydraulic diameter, $d_h = d_o - d_i$, for the annular duct the Reynolds (Re) number is defined as

$$\mathrm{Re} = \frac{w d_h \rho}{\eta} = \frac{w d_h}{\nu} \tag{3}$$

The Schmidt (Sc) and Prandtl (Pr) numbers describe the ratio of impulse to mass and heat transport, respectively

$$\mathrm{Sc} = \frac{\eta}{\rho D} = \frac{\nu}{D} \tag{4}$$

$$\mathrm{Pr} = \frac{\eta c_P}{\lambda} = \frac{\nu}{a} \tag{5}$$

In the case of laminar flow ($\mathrm{Re} < 2300$), at the beginning of the module, neither temperature, concentration, nor hydrodynamic profile is developed, whereas at the end of the membrane all profiles are fully developed. Hence, an approximation of the average Nu and Sh numbers, including the influence of inlet effects, has to cover the complete range from hydrodynamically (1) over thermally (2) developing through to developed (3) flow

$$\mathrm{Nu} = (\mathrm{Nu}_1^3 + \mathrm{Nu}_2^3 + \mathrm{Nu}_3^3)^{1/3} \tag{6}$$

with

$$\mathrm{Nu}_1 = \left(\frac{2}{1 + 2\,\mathrm{Pr}}\right)^{1/6} \left(\mathrm{Re}\,\mathrm{Pr}\,\frac{d_h}{l}\right)^{1/2} \tag{7}$$

$$\mathrm{Nu}_2 = 1.615 \left\{1 + 0.14 \left(\frac{d_i}{d_o}\right)^{-1/2}\right\} \left(\mathrm{Re}\,\mathrm{Pr}\,\frac{d_h}{l}\right)^{1/3} \tag{8}$$

$$\mathrm{Nu}_3 = 3.66 + 1.2 \left(\frac{d_i}{d_o}\right)^{-0.8} \tag{9}$$

In the turbulent flow regime ($\mathrm{Re} > 2300$) the following function is derived in dependency on the flow in tubes:

$$\mathrm{Nu} = 0.86 \left(\frac{d_i}{d_o}\right)^{-0.16} \frac{\frac{\xi}{8} \cdot (\mathrm{Re} - 1000)\mathrm{Pr}}{1 + 12.7 \sqrt{\frac{\xi}{8}} \cdot (\mathrm{Pr}^{2/3} - 1)} \left\{1 + \left(\frac{d_h}{l}\right)^{2/3}\right\} \tag{10}$$

with the friction factor for turbulent tube flow according to

$$\xi = (1.82 \log_{10}\mathrm{Re} - 1.64)^{-2} \tag{11}$$

The temperature dependency of the physical properties may be included by

$$\mathrm{Nu} = \mathrm{Nu}_M \left(\frac{\mathrm{Pr}}{\mathrm{Pr}_M} \right)^{0.11} \tag{12}$$

Calculation of the pressure drop in the porous support

Any theoretical study of permeation through porous materials begins with the comparison of the mean free path of the molecules λ and the average pore size d_p of the structure. The mean free path is connected over geometrical relations to the kinetic diameter of the permeating molecules

$$\lambda = \frac{kT}{\sqrt{2}\, p d_{kin}^2 \pi} \tag{13}$$

If the mean free path of the molecules is much smaller than the pore size the dominant flux mechanism is viscous flow with molecule–molecule collisions. If the mean free path is much greater than the pore size, Knudsen diffusion with molecule–wall interactions is the dominant mechanism. The Knudsen number (Kn) provides a good measure on the prevailing effect.

$$\mathrm{Kn} = \frac{\lambda}{d_p} \tag{14}$$

For $\mathrm{Kn} > 10$ the transport occurs exclusively by Knudsen diffusion, whereas for $\mathrm{Kn} < 10^{-2}$ viscous flow is the predominant mechanism. In the transition regime from $10^{-2} < \mathrm{Kn} < 10$ both effects contribute to the overall permeation through the support. For permeation through an isotropic support with cylindrical and straight pores the two extreme cases, Knudsen diffusion and viscous flow, can be described by[39]

$$J_i^{\mathrm{Kn}} = \frac{2 d_p \varepsilon_{sup}}{3 \tau_{sup}} \sqrt{\frac{2M_i}{\eta_i RT}} \frac{\Delta p}{\delta_{sup}} \tag{15}$$

$$J_i^{vis} = \frac{d_p^2 \varepsilon_{sup} M_i \bar{p}_i}{32 \tau_{sup} \eta_i RT} \frac{\Delta p}{\delta_{sup}} \tag{16}$$

The pressure drop of Knudsen diffusion is independent of the absolute pressure, whereas for viscous flow the specific pressure drop increases with decreasing pressure level. In the transition regime and for a real pore structure, where both mechanisms occur in parallel (size distribution) and in series

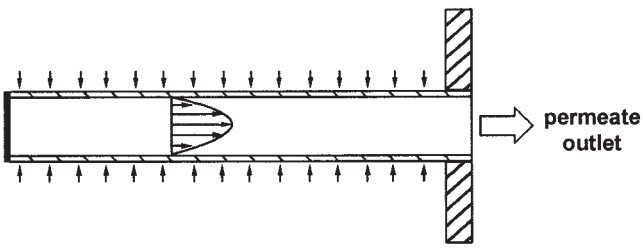

Figure 3. Permeate flux and flow conditions inside a tubular membrane.

Table 1. Permeance and Activation Energy of IPA and Water for Pervaporation with Amorphous Silica Membranes at a Reference Temperature of 80°C*

Compound	Permeance Q_{ref} (kg m^2 hbar^{-1})	Activation Energy E (kJ/kmol)
Water	10.01	12.5
Isopropanol	0.263	12.6

*From Somer and Melin.[46]

(variable diameter in a pore system), the transport is best described by an empirical approach[39]

$$J_i = a \left(\frac{\bar{p}_i}{p_{ref}} \right)^b \Delta p_i \tag{17}$$

The parameters a and b have to be determined experimentally. The membrane permeation constant a takes the porosity ε, tortuosity τ, and pore size distribution into account. The exponent b is between 0 and 1 and indicates to which extent viscous flow or Knudsen diffusion contributes to the permeability.

Determination of the pressure gradient on the permeate side

Figure 3 shows the conditions for a single membrane tube in the module. One end is closed and the other is connected to the permeate side. The feed is assumed to be on the outside, whereas the permeate flows inside the tube.

In the simulation of the permeate pressure gradient, the continuous mass increase over the unit length has to be taken into account in a differential mass balance

$$\frac{d\dot{m}_P}{dz} = \pi d J \tag{18}$$

By assuming laminar flow in the tubular permeate channel, the pressure drop may be expressed by the differential form of the Hagen–Poiseuille equation

$$\frac{dp_P}{dz} = -\frac{128\eta}{\rho \pi d_i^4} \dot{m}_P \tag{19}$$

The boundary conditions for Eqs. 18 and 19 are $z = 0$: $\dot{m}_P = 0$ and $z = 1$: $p = p_P$. The two differential equations constitute a two-point boundary value problem attributed to the unknown permeate pressure profile inside the tube. This requires a trial-and-error method or a numerical iteration to solve the problem. For a practical solution one may suppose a constant permeate flow rate from the dead end to the outlet so that a simple analytical solution is obtained allowing a worst-case approximation of the pressure drop on the permeate side

$$\Delta p_P = \frac{64}{\mathrm{Re}} \frac{\rho}{2} \frac{1}{d_i} w^2 \tag{20}$$

Physical properties and membrane characteristic

The physical properties of the feed and permeate mixture such as density, viscosity, diffusion coefficient, thermal con-

Table 2. Basic Design and Operation Parameters for the Simulations

Variable	Unit	Value
Process Parameter		
Feed temperature	°C	140
Permeate pressure	mbar	20
Feed flow rate	m^3/h	0.6
Feed concentration water	% wt	10
Module Geometry		
Inner membrane diameter	mm	8
Outer membrane diameter	mm	14
Membrane length	mm	760
Number of membranes	—	30
Membrane area	m^2	1
Tube diameter	mm	25
Channel diameter	mm	11

ductivity, heat capacity, heat of vaporization, vapor pressure, and activity coefficient have been calculated from tabulated values. They are correlated with empirical functions for concentration, temperature, and pressure dependencies.[40-44]

The membrane characteristics of the microporous silica membrane were incorporated into the simulation by a simple transport equation. The partial fluxes were determined for the respective operating conditions with a permeance model based on the sorption–diffusion model with an Arrhenius term for the temperature dependency[45,46]

$$J_{i,PV} = Q_i \Delta p_{i,PV} = Q_{i,ref} \exp\left[\frac{E_i}{R}\left(\frac{1}{T_{ref}} - \frac{1}{T_F}\right)\right](x_{iF}\gamma_i p_{iF}^0 - y_{iP}p_P) \tag{21}$$

The dehydration of isopropanol (IPA) by pervaporation was chosen as the model system. The necessary values of the permeance and activation energy for IPA and water in the model are listed in Table 1 for a reference temperature of 80°C.[46]

Fundamental model parameters

Different sets of simulations are carried out to understand the impact of different design and operation parameters on the process. In Table 2 the basic parameters of the various calculations are summarized. In general all simulations were made for the 30 membranes in the 1-m^2 module arranged in series. According to the deflection of the feed stream, permeate flow direction consists of alternating co- and countercurrent toward feed flow direction.

Validation of the model

The simulation model, describing the mass and heat transfer in an annular-duct tubular membrane module, was validated with pressure drop measurements and pervaporation permeation data on flux and selectivity.[13,47] Figure 4 shows that the values calculated by the program were in good agreement with the experimental data. Additionally, the results obtained with empirical correlations were compared to detailed modeling with computational fluid dynamics using the software code CFX 4.2® from AEA Technology.[13,48] Again, both calculations were in good agreement.

Performance criteria

The most important criterion for the evaluation of different concepts, geometries, and operation conditions is the average module efficiency ζ, defined as actual flux divided by ideal flux in the absence of any transport resistances

$$\zeta_{tot} = \frac{J_{tot,real}}{J_{tot,ideal}} \quad \text{or} \quad \zeta_i = \frac{J_{i,real}}{J_{i,ideal}} \tag{22}$$

Figure 5 shows the difference of the module efficiency when using the partial water flux compared to the total permeate flux for the calculation. With decreasing water feed concentration, the water flux decreases linearly whereas the organic flux stays constant, leading to a reduced permeate purity. The concentration gradient from the bulk feed to the membrane surface becomes smaller as a result of the lower selective water flux. However, this does not necessarily result in reduced concentration polarization. Therefore, the module efficiency should always be determined with the flux of the target compound in the permeate.

To allow an effective use of the installed membrane area the module efficiency should be as high as possible. The ideal case of 100% is a theoretical value that cannot be achieved in real applications. It is important to consider that for every efficiency improvement a certain expenditure has to be accepted. This has to be paid either by higher investment cost resulting from a

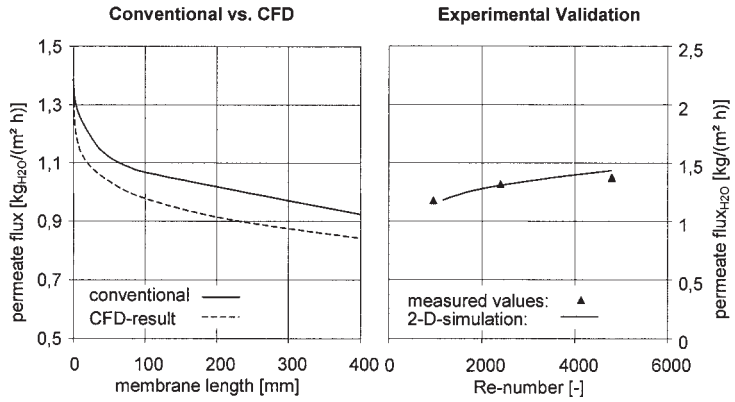

Figure 4. Validation of the model by CFD (left)[13,47] and experimental results of ECN (right).

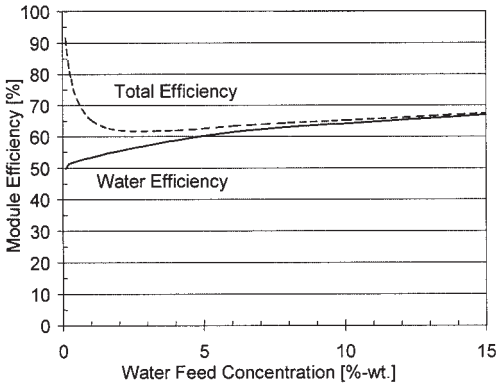

Figure 5. Difference of the definition of the module efficiency with partial water flux (solid line) and total permeate flux (dashed line).

more complex and costly module construction or with increasing operation cost arising from a higher pressure drop.

Discussion of Relevant Transport Resistances

The resistance-in-series model has been used by several authors to quantify mass and heat transport in pervaporation.[10,11,49,50] The model assumes that the transport through the membrane, which occurs in a number of consecutive steps, can be described by a series of resistances. In this study transport resistances, such as polarization effects on the feed side, axial temperature decline, and pressure drop in the porous support and permeate channel, are discussed. Concentration polarization in the porous support and axial back-mixing on the permeate side are of minor importance according to calculations by Klatt.[16] Interfacial effects, which are described by Barrer[51] for the sorption and desorption in zeolite membranes, have been neglected in this case for amorphous silica membranes.

Concentration- and temperature polarization on the feed side

Even though the so-called phenomena of concentration and temperature polarizations can be explained by different reasons, they can be described mathematically with symmetric equations. Concentration polarization is caused by the selectivity of the membrane. The rejected compounds of the feed mixture accumulate at the membrane surface, whereas the preferentially permeating compounds deplete from the bulk toward the membrane. The principle of concentration polarization is shown in Figure 6. Temperature polarization is a consequence of the phase transition of the permeate. The necessary heat of vaporization is taken from the latent heat of the feed stream. Thus, a temperature gradient develops from the bulk feed to the rear side of the membrane where the evaporation takes place.

The module efficiency, defined as flux achieved in the technical module divided by the membrane flux under ideal feed flow conditions, is shown in Figure 7 for an annular duct–type module in alcohol dehydration. The average performance decreases with increasing ideal permeate flux, from 83% at 1 kg m^{-} h^{-1} to 58% at 4 kg m^{-} h^{-1} and 42% at 8 kg m^{-} h^{-1}, for a feed flow rate of Re = 2300.[13] One third of the efficiency loss

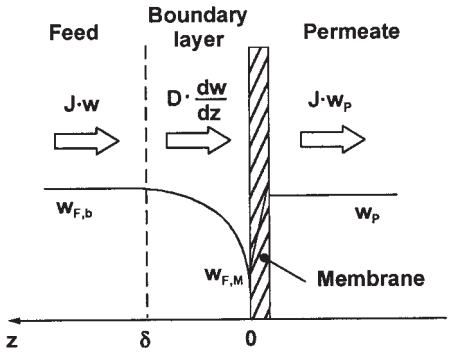

Figure 6. Principle of concentration polarization.

results from temperature polarization; the other two thirds are attributed to concentration polarization effects. This comparison clearly demonstrates why for low-flux polymeric membranes at moderate temperatures polarization effects are of minor interest. In contrast, for high-flux inorganic membranes it is a major concern, especially at elevated feed temperatures. Thus, adequate hydrodynamic design and operation are crucial for efficient modules in pervaporation. The loss of separation performance resulting from concentration and temperature boundary layers can be minimized by higher flow rates and Re numbers on the feed side. A look at the steep efficiency increase at Re = 2300 in Figure 7 shows that it is important to operate the module in the turbulent flow regime. Of course, this efficiency increase is bought by higher pumping costs arising from a corresponding pressure drop increase.

On the one hand, a comparison of parallel and perpendicular feed flow shows that the latter is more effective at the same Re number. On the other hand, however, annular duct–type modules can be operated with higher flow velocities and thus larger Re numbers at the same pressure drop. It is difficult to favor one of these designs. For pervaporation the directly heated module with parallel flow in an annular gap might be better, whereas for the isothermal vapor permeation the shell-and-tube design with baffles could be advantageous because of the high feed volumes in the vapor phase.

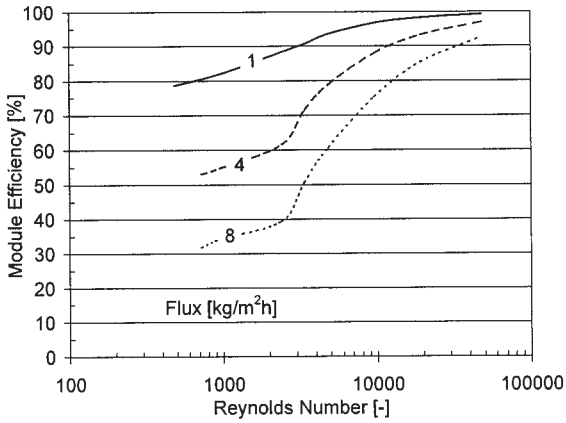

Figure 7. Calculated efficiency of an annular duct type technical module as a function of the Re number for different permeate fluxes.

Solid line: 1 kg m^{-2} h^{-1}; dashed line: 4 kg m^{-2} h^{-1}; dotted line: 8 kg m^{-2} h^{-1}.[13]

Also the physical properties of the feed mixture and the adsorption behavior of water on the membrane in different systems must be considered. The viscosity of the systems has a major impact on the transport resistances in the module. At a temperature of 20°C the viscosity is 0.89 Pa·s for water, 2.43 Pa·s for IPA, only 0.32 Pa·s for acetone and MEK, but 20.41 Pa·s for ethylene glycol and even 68.02 Pa·s for cyclohexanol.[37] Thus, differences of the dynamic viscosity between the solvents up to a factor of 100 have a significant effect on the denominator in the Re number. As a consequence this may entail considerable variations up to more than 50% in the flux performance. The water adsorption on zeolites follows a Langmuir isotherm, whereas for silica it is in the Henry region[52-57]; thus, concentration polarization effects for the latter are more severe. In this case the water adsorption coverage and thus the driving force decreases to a greater degree at the same concentration gradient from the bulk to the membrane surface.

Axial temperature decline in the module

The heat transfer in pervaporation was investigated by several researchers.[58,59] The temperature drop of the feed liquid during pervaporation as a function of flow rate, concentration, and permeate pressure was studied by Ito et al.[60] In pervaporation the evaporation of the permeate is an essential step. The corresponding heat flux is

$$\dot{q} = \sum J_i(h_{Pi} - h_{Fi}) \approx \sum J_i \Delta h_i^{LV} \tag{23}$$

This is usually drawn from the feed and is necessary for the phase change at the membrane surface to the permeate compartment. The temperature profiles develop both orthogonal to the membrane and in the axial flow direction. The temperature gradient for the heat transport orthogonal to the membrane is called temperature polarization

$$\dot{q} = \alpha_{tot} \Delta T \tag{24}$$

$$\frac{1}{\alpha_{tot}} \approx \frac{1}{\alpha_F} + \frac{\delta_M}{\lambda_M} \tag{25}$$

The heat transfer coefficient on the feed side α_F can be estimated for a given module geometry and hydrodynamics based on proven heat transfer equations. Finally, the ratio of thermal conductivity λ_M and the membrane thickness δ_M must be determined experimentally. With high-performance membranes and high driving forces the heat transport can become the rate-limiting step, especially when water with its high specific heat of evaporation is the preferentially permeating component. Thus, for the pervaporation of water/IPA mixtures through asymmetric CA membranes, temperature differences of up to 4.5 K have been measured.[58] The temperature difference between feed and permeate is irrelevant with low fluxes and organics, given that permeating species are characterized by a relatively low heat of evaporation.

However, the temperature decline in axial flow direction always has to be taken into account. The temperature difference between module inlet and outlet follows from the energy balance, neglecting heats of mixing. For $T_P \sim T_R$, $\Delta h^{LV} \neq f(T)$ and $c_{pi} \neq f(T)$ to

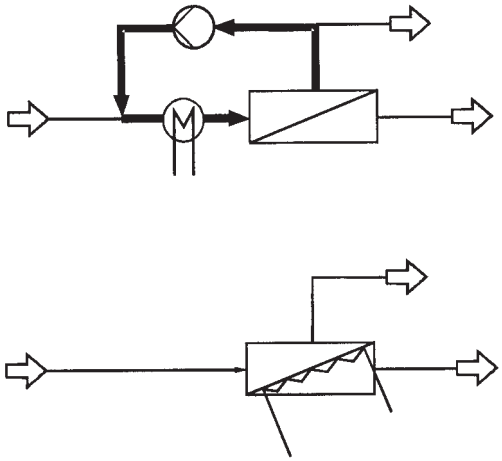

Figure 8. Different operation modes of pervaporation modules with recirculation loop or direct heating.

$$\Delta T = T_F - T_R = \frac{\dot{m}_P \Delta h^{LV}}{\dot{m}_F c_{pF}} \tag{26}$$

Because of the strong dependency of the driving force on the feed temperature the axial temperature decline in the feed has to be compensated for. Usually, this is realized by an alternating modular setup of pervaporation modules and interstage heat exchangers between them. This design leads to a rather complex installation, making pervaporation a costly process.

For each application there is a characteristic feed flow rate per membrane area to achieve a certain separation, according to Brüschke[26]

$$A = \frac{\dot{m}_F}{J_i} \ln\left(\frac{w_F}{w_R}\right) \tag{27}$$

To meet the polarization and axial temperature decline problem the feed flow rate can be increased. Thus, with higher flow velocities a partial recirculation of the product stream is required to be mixed with fresh feed. The concept is visualized in Figure 8. The internal loop to minimize the axial temperature drop causes a reduction of the feed concentration, leading to a diminished use of the membrane area. Furthermore, large recirculation streams cause a higher energy demand for the operation of the additional pumps.

In dehydration applications with high feed water concentrations, however, the modular configuration with heat exchangers and recirculation streams is often not sufficient to compensate for the temperature drop per module. Molter and Heinzelmann[61] reported that for the removal of water from 50 to 4 wt % in an industrial effluent stream, 300 m^2 instead of 60 m^2 would be needed in five recirculation steps because of the cooling effects. They suggest operating tubular pervaporation modules as a natural-circulation evaporator to reach higher efficiencies. This technology has been tested on a pilot scale at CM Celfa.[15]

Another option consists of novel isothermal pervaporation modules, which do not need a recirculation stream because of direct heating of the feed mixture, as shown in Figure 8. This

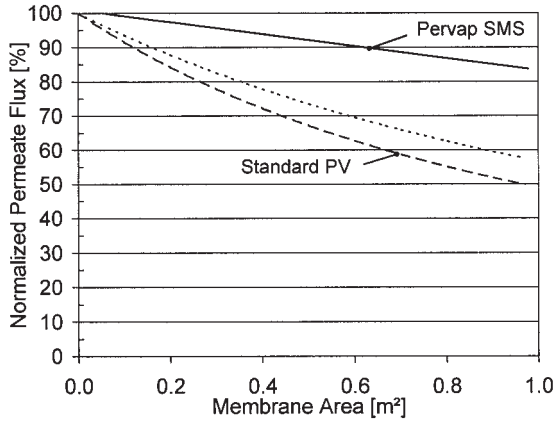

Figure 9. Flux decrease because of temperature and concentration decline in axial feed flow direction as a function of the membrane area.

Concentration (solid line), temperature (dotted line), and both effects together (dashed line).

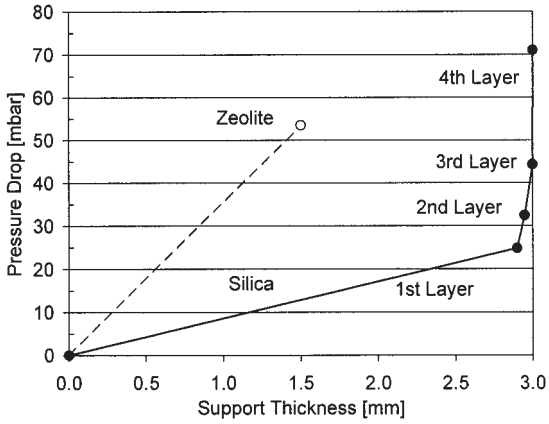

Figure 10. Development of the pressure drop over the porous support from the permeate to the feed side for the zeolite (dashed line) and the silica (solid line) membrane.

type of module has been developed by Sulzer Chemtech[14] together with ECN[25] and is now commercially available under the brand name Pervap® SMS.

The various operation modes have a strong impact on the module performance. The normalized permeate flux is compared in Figure 9 for standard adiabatic and isothermal pervaporation. In the case of a constant feed temperature, the decline in linear flux along the process train occurs just based on the desired decrease in feed concentration. In operation without heating there is an additional decrease in exponential flux from the inlet to the outlet caused by the temperature drop. At the end of a module with a membrane area of 1 m^2 the flux reduction attributed to decreasing concentration is 17.1%, whereas the temperature drop lowers the permeation rate by 42.5%. Thus, 82.9% of the initial flux level remains with isothermal operation, whereas in the adiabatic case the value is only 49.8%. This effect becomes even more pronounced with larger membrane areas. The effect of interstage to isothermal operation is compared elsewhere for a full-size IPA dehydration plant.[62]

Influence of the porous support

For tubular zeolite and silica membranes there are different requirements for the porous support. Besides the necessity of providing sufficient mechanical strength, the support should allow the application of a thin and defect-free separation layer on top. The thermal crystallization of zeolites tolerates larger pore sizes and greater surface roughness than the preparation of amorphous silica layers by sol–gel processing. Hence, the zeolite membrane from Mitsui[24] contains just one alumina support layer, whereas the silica membrane from ECN[25] consists of an asymmetric structure with a total of four layers. The features of the two supports are listed in Table 3.[63,64]

By taking the pore dimensions and permeate operating conditions of pervaporation into account, one may assume Knudsen diffusion to be the predominant transport regime according to Rautenbach et al.[65] The development of a pressure drop over the porous support is compared in Figure 10 for the two membranes at a pure water permeate flux of 6 kg m^{-} h^{-1} at a temperature of 90°C and a permeate pressure of 10 mbar.

The pressure drop in the zeolite membrane support is 53 mbar and slightly smaller than in the porous structure of the silica membrane with 71 mbar. The increase of the pressure drop with the distance is inversely proportional to the ratio of tortuosity and porosity, and the pore size according to Eq. 15. In the α-Al_2O_3 layer of the ECN membrane, the different gradients are attributed to the varying pore diameters because the ratio of tortuosity to porosity of 4 is the same. Because of the large thickness of the first layer the pressure drop is 25 mbar. For the much thinner second and third layers it is still 8 and 12 mbar as a result of the reduced pore size. The highest friction loss occurs in the fourth layer with 27 mbar. The ratio of tortuosity to porosity of the γ-Al_2O_3 layer is 5 but the pore

Table 3. Features of the Support Layers of the Amorphous Silica Membrane from ECN and the Zeolite Membrane from Mitsui*

	Membrane Support Silica				Zeolite
Feature	1st Layer	2nd Layer	3rd Layer	4th Layer	Mullite Layer
Material	α-Al_2O_3	α-Al_2O_3	α-Al_2O_3	γ-Al_2O_3	$3Al_2O_3 \cdot 2SiO_2$
Thickness	3 mm	50 μm	50 μm	2 μm	1.5 mm
Pore size	5 μm	0.28 μm	0.18 μm	4 nm	1 μm
Porosity	0.35	0.35	0.35	0.60	0.40
Tortuosity	1.4	1.4	1.4	3	2

*From Kondo et al.[63] and Alderliesten.[64]

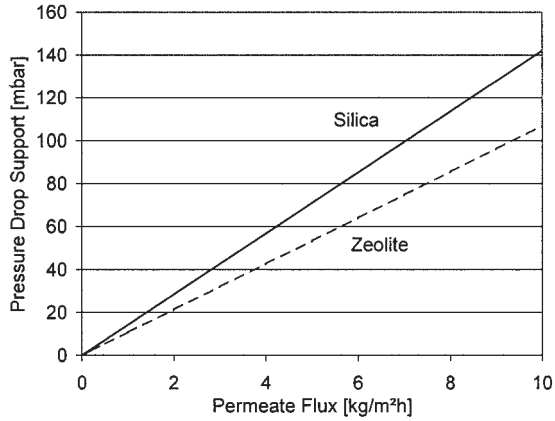

Figure 11. Impact of the total permeate flux on the pressure drop in the porous support for the zeolite (dashed line) and the silica (solid line) membrane.

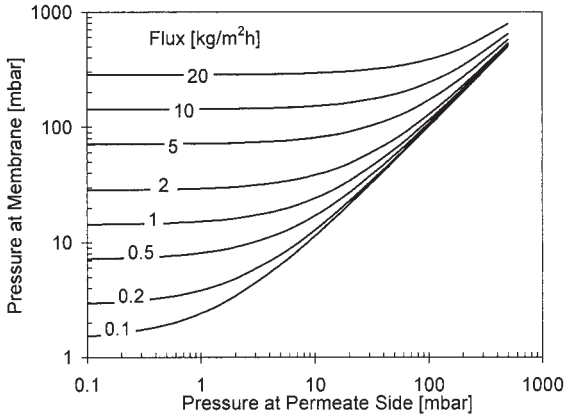

Figure 12. Effect of the permeate pressure level and the total permeate flux on the pressure drop in the porous support of the silica membrane.

diameter is only 5 nm, which leads to the steep rise in such a short distance.

The development of improved porous supports for inorganic pervaporation membranes has to aim at achieving small friction losses. The main parameter to manipulate is the layer thickness because porosity and tortuosity are usually determined by the material and a stepwise reduction of the pore size is needed to prepare defect-free membranes.[66,67] The pressure drop in the porous support can be minimized by a reduction of the thickness with the preparation of capillaries and hollow fibers. However, because of the overall smaller dimensions of the permeate channels the pressure drop inside the fiber increases.

The pressure drop increases linearly with the permeate flux, as shown in Figure 11. The estimation of the pressure drop, assuming pure Knudsen diffusion, demonstrates that at high fluxes an excessive reduction in driving force has to be accepted. This is attributed to friction losses and can be easily tolerated. As a result of dehydration in the ppm region, where very small driving forces and thus low fluxes prevail, hardly any pressure drop will be observed.

In the area of low concentrations another effect, often called internal sweep, sustains the permeate flux. In dehydration applications, for example, the partial pressure of water in the permeate is reduced with decreasing water flux because of the constant small organic flux. With the lower permeate purity the decrease in driving force decelerates. Thus, one may regard this effect as a self-regulating system. An interesting question in this context concerns the location of the permeate evaporation. Depending on the pressure drop this place may not be directly at the rear side of the active layer but it is conceivable that the position shifts to somewhere in the porous support.

A matrix of the various parameters is visualized in Figure 12, to summarize the effect of permeate pressure level and total permeate flux on the pressure drop in the porous support of the silica membrane. The calculations demonstrate that there is a minimum pressure at the rear side of the active layer for a given permeate flux, independently of the pressure applied in the permeate channel by the condensation level and vacuum pump.

Pressure drop in the permeate piping

The packing density of tubular membrane modules is generally limited to 100 m^2/m^3. The value can be increased to more than 1000 m^2/m^3 by the use of capillary or hollow-fiber membranes with smaller dimensions. Voigt et al.[32] compared the membrane area of single sealed mono-channel tubes with different bundle-plotted capillary geometries. The modules were of 1 m length and various diameters. Table 4 shows the impressive increase of the membrane area.

The pressure buildup in shell-side feed hollow-fiber pervaporation membrane modules has been intensively studied by Rautenbach and Albrecht[58] as well as Feng and Huang.[68] Both studies found that the membrane performance at the dead end of the fiber can be reduced to under 30% of the value at the open side. With increasing tube/fiber diameter the pressure drop in the permeate channel is of less importance, whereas the corresponding packing density decreases. Module optimization must be aimed toward the maximization of the permeate yield. For each fiber length there is an optimal diameter tending to larger values for longer fibers. The efficiency of hollow-fiber modules increases with shorter fiber length but they should not be too small for economical reasons of module manufacturing. A typical length is around 0.5 m.[19] The calculations of both groups[58,68] revealed that the optimal inner fiber diameter for the low-flux polymeric membranes investigated was around 0.5 mm. As a rule of thumb for high-flux inorganic membranes, with permeation rates up to 10 kg m^{-} h^{-1}, the inner fiber diameter should not fall below 2 mm.

The pressure drop in the amorphous silica membranes from ECN (length: 800 mm; OD:14 mm; ID: 8 mm) was calculated

Table 4. Packing Density of Modules with Tubular Membranes of Different Geometry

	Membrane Dimension (OD/ID) (mm)		
Module Diameter (mm)	10/7	2.8/2	1.1/0.5
30	0.022	0.55	0.84
50	0.066	1.3	2.5
100	0.42	6.3	11
200	1.3	26	45

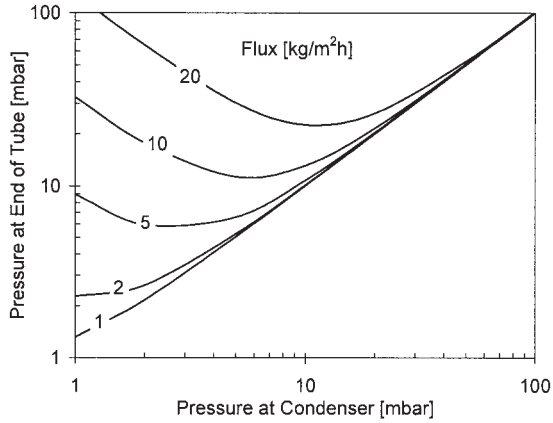

Figure 13. Effect of the permeate pressure level and the total permeate flux on the pressure drop in the permeate tube of the silica membrane.

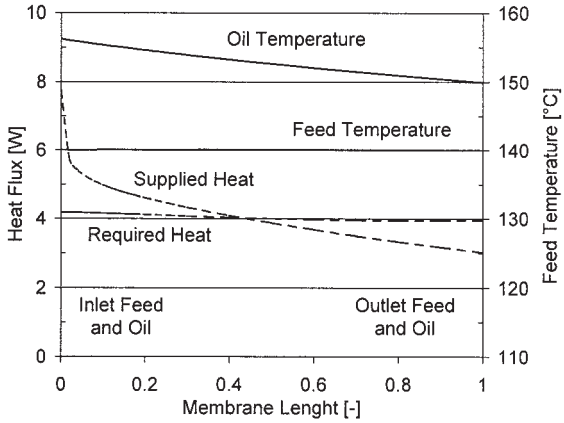

Figure 15. Temperature (solid line) and heat flux (dashed line) over the membrane length for thermal liquid heating with cocurrent flow.

with laminar permeate flow according to Hagen–Poiseuille. The permeate pressures at the dead end of the tube are plotted over the pressure applied in the condenser in Figure 13 for several permeate flux rates. It is shown that decreasing the permeate pressure below 10 mbar does not lead to an increase in performance. Because of the compressibility the pressure drop in gas and vapor flow is inversely proportional to the pressure level.

Isothermal Operation of the Pervap® SMS Module

For the choice of the heating medium, the operation temperature of the module in a certain application has to be taken into account. Because of the pressure stage of the stainless steel design, a maximum of 16 bar may not be exceeded. Thus, the use of steam condensation is limited up to a maximum of 200°C. For operation temperatures above this value a suitable thermal liquid has to be selected to transfer the necessary heat. The design principle of the shell-side heating is shown in Figure 14.

The flow direction in the heat exchanger is a cross-current pattern superposed by alternating co- and countercurrent flow with respect to the feed stream. In the simulation the steam heating was modeled by means of film condensation with a constant wall temperature. The operation with thermal oil was simplified to co- and countercurrent flows, respectively, because the programming effort would have been too large otherwise. This procedure was proven to be practical, given the negligible differences between the calculated results.

The profiles of temperature and heat flux for the heat supply with thermal liquid are given in Figure 15 for cocurrent flow and in Figure 16 for countercurrent flow.

The heat transfer is best at the feed inlet because of entrance effects. The feed temperature is not exactly uniform over the whole module. At the inlet, where the feed concentration and thus permeate flux are high, a strong cooling results in a somewhat lower operation temperature. Toward the outlet the feed temperature rises again because of the reduced flux. The heat balance for one membrane in the module for cocurrent flow is positive in the beginning and then negative, whereas for countercurrent flow the supplied heat is lower than the required heat at the inlet of the annulus and higher at the outlet. The effect on the feed temperature, however, is negligible.

The hydrodynamics and the temperature profile in the annu-

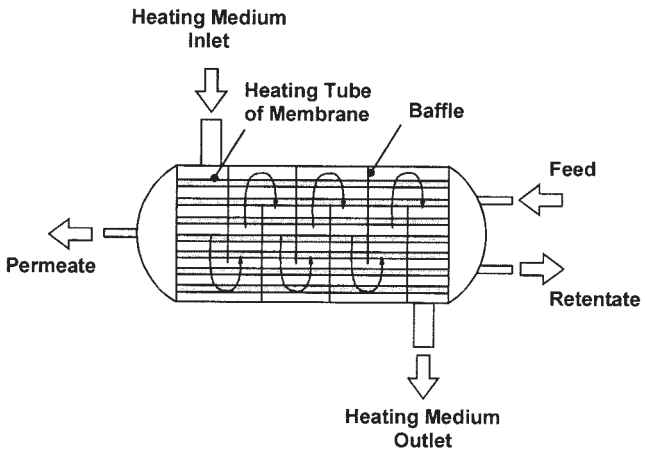

Figure 14. Principle design of the shell-and-tube heat exchanger in the Pervap® SMS module.

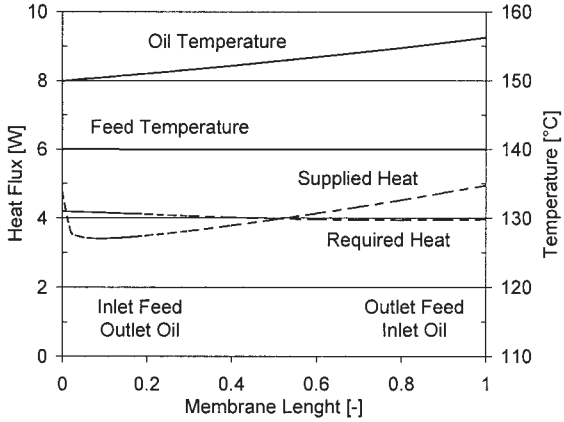

Figure 16. Temperature (solid line) and heat flux (dashed line) over the membrane length for thermal liquid heating with countercurrent flow.

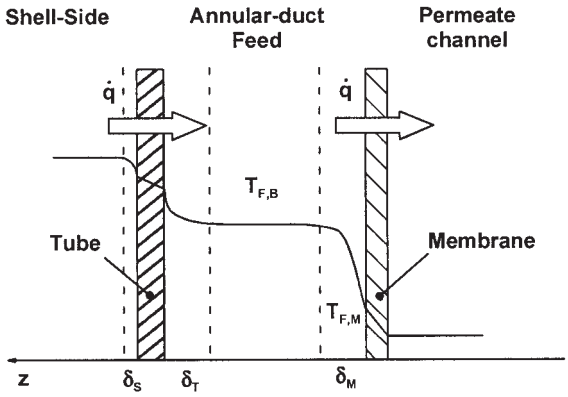

Figure 17. Flow pattern and temperature profile in the annular duct from the heat-exchanger tube to the membrane.

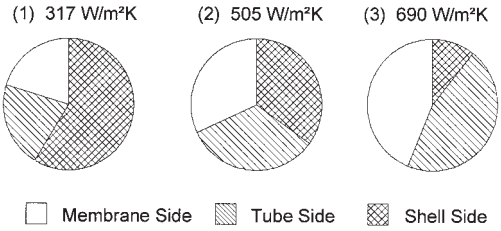

Figure 19. Composition of the overall heat transfer coefficient from the resistances in the single boundary layers for different heating principles.

(1) Thermal liquid with 2 m^3/h, (2) thermal liquid with 10 m^3/h, (3) steam condensation.

lar gap are shown schematically in Figure 17. In the turbulent bulk of the feed stream the temperature is nearly constant. On the membrane side and the tube side of the feed channel there are laminar boundary layers, implying a temperature gradient. Another orthogonal temperature profile exists on the shell side of the tube.

For the operation with thermal liquid the energy supply and transport can be adapted by the oil flow rate to every required energy demand, as can be seen from Figure 18. Only pumping capacity, module construction, and thermal resistance may be the limiting factors. The shell-side heat transfer coefficient increases with the oil flow rate. The reduced boundary layer thickness at higher Re number involves a lower resistance. Furthermore, at a higher flow rate a larger amount of heat energy is transported with the heat capacity of the oil. Both effects lead to a reduction of the temperature difference from the oil inlet to the outlet to achieve an isothermal operation.

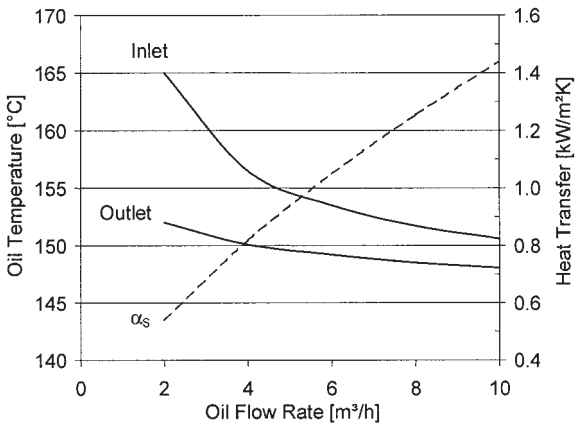

Figure 18. Inlet and outlet oil temperature and shell-side heat transfer coefficient as function of the oil flow rate for the use of thermal liquid in the module.

The major performance difference between the heating modes emerges on the shell side of the tube. As shown in Figure 18 the shell-side heat transfer coefficient for oil heating increases from 540 W m^{-2} K^{-1} at 2 m^3/h to 1440 W m^{-2} K^{-1} at 10 m^3/h, whereas the temperature gradient decreases from 12.9 to 4.8 K. In comparison the heat transfer by steam condensation is greater by up to one order of magnitude. The heat transfer coefficient is as high as 6540 W m^{-2} K^{-1} with a temperature gradient of only 1.1 K. The values were taken at the isocaloric point where the supplied heat and required heat are in balance.

Heat transfer coefficients together with the temperature gradients in the different boundary layers are listed in Table 5 for various heating modes and parameters. To better visualize the proportions, the corresponding heat transfer resistances—the contribution of each single barrier and the overall amount—are plotted as pie diagrams in Figure 19.

Because the operation parameters on the feed side do not change, heat transfer and hydrodynamic conditions are the same for all cases. In the annular duct the heat transfer coefficient on the membrane side is around 1570 W m^{-2} K^{-1}, with a temperature difference of 7.7 K from the bulk to the surface. The heat transfer coefficient on the tube side of the feed channel is around 1520 W m^{-2} K^{-1}, with a temperature gradient of 4.5 K from the bulk to the tube. The deviation arises from the varying heat transfer areas in the feed gap with an inner diameter of 14 mm at the membrane side and an outer diameter of 25 mm at the tube side. The overall heat transfer resistance is obtained by adding the reciprocal values of the heat transfer resistances in the various boundary layers. The

Table 5. Heat Transfer Coefficients and Temperature Gradients for Various Heating Modes and Parameters

	Membrane Side		Tube Side		Shell Side	
Heating Mode	α_M (W m^{-2} K^{-1})	ΔT (K)	α_T (W m^{-2} K^{-1})	ΔT (K)	α_S (W m^{-2} K^{-1})	ΔT (K)
Thermal Liquid						
Oil flow rate 2 m^2/h	1565	7.8	1510	4.6	540	12.9
Oil flow rate 10 m^3/h	1580	7.7	1530	4.5	1440	4.8
Steam condensation	1575	7.7	1520	4.3	6540	1.1

Table 6. Field of Sensitivity Study to Determine the Influence of Design and Operation Parameters on the Module Performance

Parameter	Unit	Value
Membrane characteristic		
Water permeance	(kg m^{-2} $hbar^{-1}$)	1–100
Module geometry		
Feed temperature	°C	100–150
Feed flow rate	m^3/h	0.4–1.2
Feed concentration water	% wt	0.1–15
Module geometry		
Tube diameter	mm	17–25
Channel diameter	mm	3–11

overall heat transfer coefficient increases from 317 and 505 W m^{-2} K^{-1} for an oil flow of 2 and 10 m^3/h, respectively, to 690 W m^{-2} K^{-1} for heating with steam. Thus, the share of the shell-side resistance in the total heat transfer resistance to the membrane decreases from 58.7 to 35.1% for the two extreme cases investigated for oil heating and just 10.6% for steam condensation. Altogether, the heat transfer by steam condensation is 50 to 100% better than using a thermal liquid.

An isothermal operation of the module is viable with both steam condensation and a liquid heat medium. Because of the higher heat transfer coefficient steam is the preferred heating medium. In addition, a modulation of the steam supply to the required heat demand can be easily accomplished.

Performance Limitation of the Pervap® SMS Module

The influence of operation and design on the performance was evaluated for a number of parameters such as concentration, temperature, flow rate, membrane permeance, and annular duct diameter. In each calculation only one variable was modified, whereas the other remained unchanged at their base value given in Table 2. An overview on the parameter range of the sensitivity study is listed in Table 6.

Depending on the application either the heat or mass transport can be the limiting factors for the module efficiency. On the one hand, for operation at high water concentrations, with hetero-azeotropes, such as water/methylisobutylketone, ethyl acetate, or *t*-butanol, there is a considerable impact of temperature polarization arising from the large heat flux necessary for the evaporation of permeate. On the other hand, for dehydration of hydrocarbons in the ppm region, such as hexane or toluene, the influence of concentration polarization is much more important. In this case the small availability of water molecules in the bulk stream leads to a complete depletion at the membrane surface. These phenomena are reflected by the impact of water permeance and feed concentration on the separation.

The effect of the feed concentration on temperature and concentration polarizations as well as overall module performance for the separation of IPA/water is shown in Figure 20. The module efficiency increases from 0.1 to 15.0 wt % water in the feed from 51.2 to 66.9%. The superior performance is also connected with a change of the physical properties of the feed mixture such as viscosity and density. From the small to the high water content the influence of temperature polarization increases from 10.9 to 48.9%, whereas the effect of concentration polarization decreases from 89.1 to 51.1%.

At low feed concentrations of water the permeation rate is small. Thus, not much heat is needed for the evaporation of permeate and the impact of temperature polarization is negligible. At 0.1 wt % water and a partial flux of 0.1 kg m^{-2} h^{-1} its portion of the flux reduction is only 5.3%, whereas concentration polarization is responsible for 43.5% of the decrease. With increasing water content and higher permeation rates the influence of the temperature gradient becomes greater. At a feed concentration of 15.0 wt % and a permeate water flux of 21.0 kg m^{-2} h^{-1}, temperature polarization already accounts for 16.2% of the performance loss. With a share of 16.9%, concentration polarization is in the same order. At higher fluxes the impact of the heat transfer is even greater than the mass transfer.

Improvements in membrane development may lead to a further increase in performance. The impact of the membrane separation characteristic on the module efficiency is plotted in Figure 21 for a variation of the water permeance in dehydration of solvents. As stated earlier, at small permeances polarization effects are not an important factor in module design. For a water permeance of 1 kg m^{-2} $hbar^{-1}$ the module efficiency is still 93.0%. The flux reduction is attributed to 51.4% by temperature and 48.6% by concentration polarization. At a water permeance of 50 kg m^{-2} $hbar^{-1}$ only 28.7% of the ideal membrane flux would be obtained in a technical module. The performance loss is attributed to 32.7% from heat and to 67.3% from mass transfer. Hence, with increasing permeance the transport limitation shifts from temperature to concentration polarization.

Higher feed temperatures result in an increase of the driving force and thus a rise of the ideal membrane flux. Larger permeation rates cause an increase of concentration as well as temperature polarization to the same extent. Thus, the module efficiency decreases from 100 to 150°C from 79.2 to 60.4%, whereas the total flux increases from 5.4 to 22.6 kg m^{-2} h^{-1}.

The variation of the feed flow rate and the tube diameter have an impact on the feed velocity and the Re number. The hydrodynamics affect both mass and heat transfer. The module

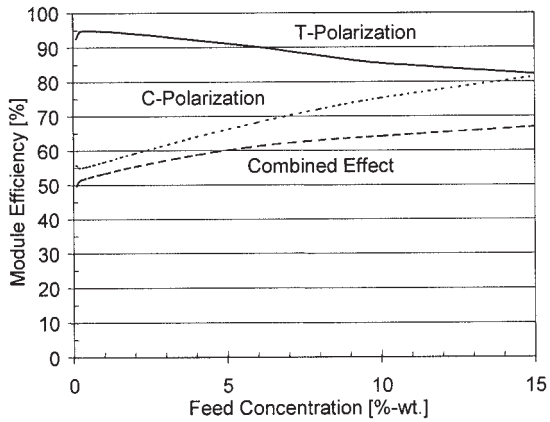

Figure 20. Influence of the feed concentration on polarization effects and module efficiency.

Concentration (dotted line), temperature (solid line), and both effects together (dashed line).

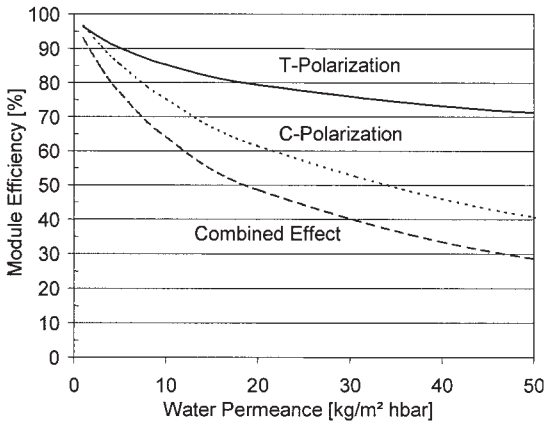

Figure 21. Temperature and concentration polarization together with the module efficiency as function of the membrane water permeance.

Concentration (dotted line), temperature (solid line), and both effects together (dashed line).

efficiency and total permeate flux increase within a feed flow rate of 0.4 and 1.2 m^3/h from 55.6 to 76.4% and 15.5 to 21.0 kg m^{-2} h^{-1}, respectively. The improvement is caused by a higher turbulence in the feed channel because of an increase of the feed velocity from 0.3 to 1.0 m/s and Re number from 9100 to 27,400. With decreasing tube diameter, between 25 and 17 mm, module performance and overall permeation rate increase from 65.2 to 87.9% and 17.8 to 23.9 kg m^{-2} h^{-1}, respectively. This is related to an increase of the feed velocity from 0.5 to 2.4 m/s and Re number from 13,700 to 17,300. The pressure drop on the feed side per membrane path without turnaround increases from 2 to 148 mbar at the same time.

Conclusions

For solvent dehydration by pervaporation with microporous inorganic membranes, tubular geometries are state-of-the-art technology. With recently available high-flux membranes, transport resistances in the shell-and-tube type modules may become a performance bottleneck. The efficiency of the isothermal module concept Pervap® SMS (Silica Membrane System) from Sulzer Chemtech was evaluated and compared to other design versions. The necessary energy for the evaporation of permeate can be supplied from the shell side to the feed mixture in an annular duct. Thus, a reduction of the permeate flux, based on an axial temperature drop, can be prevented. At temperatures above 200°C thermal liquids have to be used because of pressure stability reasons of the module design. For lower temperatures steam condensation is preferred to transfer of heat because of the smaller transport resistance. The polarization effects on the feed side can be minimized by suitable hydrodynamic design. The flow velocities can be adapted by the channel diameter to a certain feed flow rate, ensuring good mass and heat transfer and low pressure drop. Nevertheless, the reduction of the module efficiency resulting from concentration and temperature polarizations is in the range of 30 to 50%. Usually the mass transfer limitations are predominant but, depending on the application, sometimes the heat transfer plays a more important role at higher permeation rates. This essentially has to be taken into account when determining the membrane area of an industrial plant for a specific separation. Other important design criteria are friction losses in the membrane support and the permeate channel. Selectivity and flux significantly decrease in hindered permeate flows. With more than 100 mbar at a permeate flux of 10 kg m^{-2} h^{-1} the pressure drop in the support is a relevant factor for the tubular silica membrane because of the large thickness and the numerous layers. However, with a few mbar the pressure drop in the permeate tube is negligible. These values show that adequate materials and geometric design with asymmetric structures and ample cross sections are required for small flow resistances in the vacuum. To increase the packing density by more than one order of magnitude, module types such as hollow fibers and multichannel monoliths are feasible options. Their development has to consider several constraints. At fiber diameters below 2 mm the increase of the pressure drop is so steep that the advantage of the higher packing density will be sacrificed because of a pressure buildup inside the fiber. With increasing size and thus module diameter of a multichannel monolith the permeate removal through the porous support becomes a serious problem because the permeation distances become longer and the available width is very small.

Acknowledgments

We gratefully acknowledge financial support by the European Commission under the contracts JOE3-CT97-0074 and ENK6-CT1999-00015 with the following project partners: ECN in Petten, Akzo-Nobel in Arnhem (both in The Netherlands), IFP in Paris, France, and Sulzer Chemtech in Neunkirchen, Germany. We are very thankful to Mitsui Engineering & Shipbuilding, Okayama, Japan; ECN, Petten, The Netherlands for providing the membranes used in this study.

Notation

a = thermal diffusivity, m^2/s
A = membrane area, m^2
c_P = heat capacity, kJ kg^{-1} K^{-1}
d = diameter, m
D = diffusion coefficient, m^2/s
E = activation energy, kJ/kmol
h = enthalpy, kJ/kg
J = (permeate) flux, kg m^{-2} h^{-1}
k = Boltzmann constant, J/K
l = membrane length, m
$\dot{m}$ = mass flow rate, kg/h
M = molecular weight, kg/kmol
P = (partial) pressure, bar
$\dot{q}$ = heat flux, W/m^2
Q = permeance, kg m^{-2} $hbar^{-1}$
R = gas constant, kJ $kmol^{-1}$ K^{-1}
t = time, s
T = temperature, K
w = mass fraction, kg/kg
w = velocity, m/s
x = liquid molar fraction, mol/mol
y = vapor molar fraction, mol/mol
z = length coordinate, m

Dimensionless numbers

Kn = Knudsen
Nu = Nusselt
Pr = Prandtl
Re = Reynolds
Sc = Schmidt
Sh = Sherwood

Greek letters

α = heat transfer coefficient, W m^{-2} K^{-1}
β = mass transfer coefficient, m/s
δ = boundary layer thickness, m
Δ = difference
ε = porosity
γ = activity coefficient
ν = kinematic viscosity, m^2/s
λ = thermal conductivity, W/mK
λ = mean free path, m
η = dynamic viscosity, kg/ms
ρ = density, kg/m^3
τ = tortuosity
ξ = friction factor
ζ = module efficiency

Subscripts

B = bulk
F, P, R = feed, permeate, and retentate
h = hydraulic
i, j = chemical compounds
i, o = inside, outside
kin = kinetic
M = membrane
p = pore
PV = pervaporation
ref = reference
sup = support
tot = total
$tube$ = tube
α = inlet
ω = outlet

Superscripts

0 = saturation
Kn = Knudsen
LV = liquid–vapor
Ref = reference
vis = viscous

Literature Cited

1. Hickey PJ, Gooding CH. Modeling spiral wound membrane modules for the pervaporative removal of volatile organic compounds from water. *Journal of Membrane Science*. 1994;88:47-68.
2. Hickey PJ, Gooding CH. The economic optimization of spiral wound membrane modules for the pervaporative removal of VOCs from water. *Journal of Membrane Science*. 1994;92:1-17.
3. Hickey PJ, Gooding CH. Mass transfer in spiral wound pervaporation modules. *Journal of Membrane Science*. 1994;92:59-74.
4. Baker RW, Wijmans JG, Athayde AL, Daniels R, Ly JH, Le M. The effect of concentration polarization on the separation of volatile organic compounds from water by pervaporation. *Journal of Membrane Science*. 1997;137:159-172.
5. Crowder ML. Gooding CH. Spiral wound, hollow fiber membrane modules: A new approach to higher mass transfer efficiency. *Journal of Membrane Science*. 1997;137:17-29.
6. Mi L, Hwang S-T. Correlation of concentration polarization and hydrodynamic parameters in hollow fiber modules. *Journal of Membrane Science*. 1999;159:143-165.
7. Cussler EL, Crowder RO. Mass transfer resistances in hollow fiber pervaporation. *Journal of Membrane Science*. 1998;145:173-184.
8. Cussler EL, Gronda AM, Buechel S. Mass transfer in corrugated membranes. *Journal of Membrane Science*. 2000;165:177-187.
9. Lipnizki F, Field RW. Mass transfer performance for hollow fiber modules with shell-side axial feed flow: Using an engineering approach to develop a framework. *Journal of Membrane Science*. 2001; 193:195-208.
10. Lipnizki F, Field RW. Integration of vacuum and sweep gas pervaporation to recover organic compounds from wastewater. *Separation and Purification Technology*. 2001;22–23:347-360.
11. Lipnizki F, Field RW. Simulation and process design of pervaporation plate-and-frame modules to recover organic compounds from waste water. *Transactions of the Institution of Chemical Engineers*. 1999; 77A:231-240.
12. Witte S, Günther R, Hapke J. Study of the suitability of pervaporation modules for high-flow membranes by flow simulation. *Chemie Ingenieur Technik*. 2000;72:613-618.
13. Klinkhammer B, Sommer S, Melin T. Inorganic membrane module design: Modeling of fluid dynamics, Proceedings of the International Conference on Inorganic Membranes, ICIM6-2000, Montpellier, France, 2000:36.
14. Sulzer Chemtech GmbH Membrantechnik, Friedrichsthaler Straβe 19, 66540 Neunkirchen, Germany.
15. CM-Celfa Membranetrenntechnik AG, Bahnhofsstraβe, CH-6423 Seewen-Schwyz, Switzerland.
16. Klatt S. *Zum Einsatz der Pervaporation im Umfeld der Chemischen Industrie*, PhD Thesis. Aachen, Germany: Rheinisch Westfaelische Technische Hochschule (RWTH); 1993.
17. Gundernatsch W, Kimmerle K. New capillary modules for pervaporation. Heidelberg, Germany: Proceedings of 5th International Conference on Pervaporation Processes in the Chemical Industry; 1991: 259-271.
18. Bartels C, Kablaoui M, Reale J, Shah V. Industrial considerations in technology development. Ottawa, Canada: Proceedings of 6th International Conference on Pervaporation Processes in the Chemical Industry; 1992:544-553.
19. Blum S, Gutsche B, Barlage W. Membranunterstützte Batchreaktion—Konzepte und scale-up, Preprints 6. Aachen, Germany: Proceedings of Aachener Membran Kolloquium; 1997:161-178.
20. Holtmann T, Górak A. Prozessanalyse eines Membranreaktors zur Estersynthese im Technikumsmaβstab. *Chemie Ingenieur Technik*. 2002;74:818-824.
21. 2S—Sophisticated Systems Ltd., 10 Cromwell Place, South Kensington, London SW7 2JN, United Kingdom.
22. Pervatech BV, Rondweg 48, 7468 MC Enter, The Netherlands.
23. Alan Cobham Engineering Ltd., Holland Way, Blandford, Dorset DT11 7BJ, United Kingdom.
24. Mitsui Engineering & Shipbuilding, 1-1, Tama 3-chome, Tamano, Okayama 706-8651, Japan.
25. Netherlands Energy Research Foundation (ECN), Westerduinweg 3, NL 1755 LE, Petten, The Netherlands.
26. Brüschke HEA, Pex P. Isothermes Modul mit keramischen Membranen für die Pervaporation, Preprints 8. Aachen, Germany: Proceedings of Aachener Membran Kolloquium; 2001:I-117–I-126.
27. Wynn N. Dehydration with silica pervaporation membranes. *Sulzer Technical Review*. 2000:3.
28. Kalipcilar H, Falconer JL, Noble RD. Preparation of B-ZSM-5 membranes on a monolith support. *Journal of Membrane Science*. 2001; 194:141-144.
29. Brinkman HW, van Eijk JPGM, Meinema HA, Terpstra RA. Innovative hollow fiber ceramic membranes. *American Ceramic Society Bulletin*. 1999;78:12.
30. Tudyka S, Stroh N, Brunner H. Herstellung und Eigenschaften von anorganischen Hohlfasern für Membrananwendungen, Preprints 7. Aachen, Germany: Proceedings of Aachener Membran Kolloquium; 1999:439-442.
31. Hörpel G, Hying C, Kuppinger F-F. Keramische Membranfolien vereinigen die Vorteile von polymeren und keramischen Membranen, Preprints 8. Aachen, Germany: Proceedings of Aachener Membran Kolloquium; 2001:1-1–1-12.
32. Voigt I, Fischer G, Puhlfürβ P, Stahn M, Tusel GF. Full ceramic modules for high temperature gas separation and pervaporation. Montpellier, France: Proceedings of the 6th International Conference on Inorganic Membranes, ICIM6-2000; 2000:43.
33. Qi X, Akin FT, Lin YS. Ceramic-glass composite high temperature seals for dense ionic-conducting ceramic membranes. *Journal of Membrane Science*. 2001;193:185-193.
34. Velterop FM. Method of connecting ceramic material to another material. Patent No. EP 0 467 462 B1; 1994.
35. Kita H. Continuous synthesis of zeolitic membranes by microwave heating application to pervaporation and gas separation. *Book of Abstracts.* IWZMM2001, Purmerend, The Netherlands; 2001:29-32.
36. Stephan K. Wärmeübergang bei turbulenter und bei laminarer Strömung in Ringspalten. *Chemie Ingenieur Technik*. 1962;34:207-212.

37. Gnielinski V. *Wärmeübertragung im konzentrischen Ringspalt und im ebenen Spalt, VDI-Wärmeatlas*. 8th ed. Düsseldorf, Germany: VDI-Verlag; 1997:Gb.
38. Schlünder E-U. Forced convection in ducts. *HEDH Heat Exchanger Design Handbook*. Washington, DC: Hemisphere; 1983:2.5.1.
39. Schofield RW, Fane AG, Fell CJD. Gas and vapour transport through microporous membranes. I. Knudsen–Poiseuille transition. *Journal of Membrane Science*. 1990;53:159-171.
40. Gmehling J, Onken U. Chemistry data series. *Vapour–Liquid Equilibrium Data Collection*. Frankfurt, Germany: Dechema; 1977.
41. Yaws CL. *Physical Properties*. New York, NY: McGraw-Hill; 1977.
42. Reid RC, Prausnitz JM, Poling BE. *The Properties of Gases and Liquids*. 4th ed. New York, NY: McGraw-Hill; 1987.
43. Lide DR. *Handbook of Chemistry and Physics*. 76th ed. Boca Raton, FL: CRC Press; 1995.
44. Perry RH, Green DW. *Perry's Chemical Engineers' Handbook*. 7th ed. New York, NY: McGraw-Hill; 1997.
45. Sommer S, Melin T. Performance evaluation of microporous inorganic membranes in the dehydration of industrial solvents. *Chemical Engineering and Processing*. Submitted.
46. Sommer S, Melin T. Influence of operation parameters on the separation of mixtures by pervaporation and vapor permeation with inorganic membranes. *Chemical Engineering Science*. Submitted.
47. Klinkhammer B, Sommer S, Melin T, Lycklama a Nyeholt JA, van Delft YC, van Veen HM, Pex PPAC. Inorganic membrane pervaporation module design. Part 1. General concept and approach. In: Genné I, Leysen R, Schaep J, Vandecasteele C, eds. *Book of Abstracts 1*. Leuven, Belgium: Proceedings Euromembrane '99; 1999:299-300.
48. Lycklama a Nyeholt JA, van Delft YC, van Veen HM, Pex PPAC, Sommer S, Klinkhammer B, Melin T. Inorganic membrane pervaporation module design. Part 2. Optimisation by computational fluid dynamics. In: Genné I, Leysen R, Schaep J, Vandecasteele C, eds. *Book of Abstracts 1*. Leuven, Belgium: Proceedings Euromembrane '99; 1999:210-211.
49. Huang RYM, Feng X. Resistance model approach to asymmetric polyetherimide membranes for pervaporation of isopropanol/water mixtures. *Journal of Membrane Science*. 1993;84:15-27.
50. Liu MG, Dickson JM, Cote P. Simulation of a pervaporation system on the industrial scale for water treatment. Part I. Extended resistance-in-series model. *Journal of Membrane Science*. 1996;111:227-241.
51. Barrer RM. Porous crystal membranes. *Journal of the Chemical Society—Faraday Transactions I*. 1990;86:1123.
52. Shigetomi T, Nitta T, Katayama T. A model of localized and nonlocalized adsorption for the system of water and methanol in A-type zeolite. *Journal of Chemical Engineering of Japan*. 1982;15:249-254.
53. Bindal RC, Misra BM. Separation of binary liquid systems by sorption a comparison with pervaporation. *Separation Science and Technology*. 1986;21:1047-1058.
54. Yamanaka S, Malla PB, Komarneni S. Water sorption and desorption isotherms of some naturally occurring zeolites. *Zeolites*. 1989;9:18-22.
55. Carter JW, Barrett DJ. Comparative study for fixed bed adsorption of water vapor by activated alumina, silica gel and molecular sieve adsorbents. *Transactions of the Institution of Chemical Engineers*. 1973;51:75-81.
56. Adell A, Petrissans J. Gas chromatography study of the adsorption of refrigerating fluids on microporous solid adsorbents. *Talanta*. 1998; 45:777-786.
57. Wolf HE, Schlünder E-U. Adsorption equilibrium of solvent mixtures on silica gel and silica gel coated ceramics. *Chemical Engineering and Processing*. 1999;38:211-218.
58. Rautenbach R, Albrecht R. The separation potential of pervaporation. Part II. Progress design and economics. *Journal of Membrane Science*. 1985;25:25-54.
59. Karlsson HOE, Trägardh G. Heat transfer in pervaporation. *Journal of Membrane Science*. 1996;119:295-306.
60. Ito A, Feng Y, Sasaki H. Temperature drop of feed liquid during pervaporation. *Journal of Membrane Science*. 1997;133:95-102.
61. Molter B, Heinzelmann W. Verfahrens- und modultechnische Lösungen für untypische Anwendungsfälle der hydrophilen Pervaporation, Preprints 8. Aachen, Germany: Proceedings of the Aachener Membran Kolloquium; 2001.
62. Sommer S, Melin T. Design and optimization of hybrid separation processes for the dehydration of iso-propanol and other organics. *Industrial and Engineering Chemistry Research* 17, 2004:5248–5259.
63. Kondo M, Komori M, Kita H, Okamoto K. Tubular-type pervaporation module with zeolite NaA membrane. *Journal of Membrane Science*. 1997;133:133-141.
64. Alderliesten P. *Inorganic Membranes: New Solutions for Your Separation Problems*. ECN-B-96-033. Petten, The Netherlands: Netherlands Energy Research Foundation (ECN).
65. Rautenbach R, Herion C, Meyer-Blumenroth U. Engineering aspects of pervaporation: Calculation of transport resistances, module optimization and plant design. In: Huang RYM, ed. *Pervaporation Membrane Separation Processes*. Amsterdam: Elsevier; 1991.
66. Bonekamp BC. Preparation of asymmetric ceramic membrane supports for pervaporation and gas separation membranes by dip coating. In: Burggraaf AJ, Cot L, eds. *Fundamentals of Inorganic Membrane Science and Technology*. Amsterdam: Elsevier; 1999:141-225.
67. Bonekamp BC, Pex PPAC. Suspensions and sol processing for the manufacturing of high performance ceramic pervaporation and gas separation membranes. *Industrial Ceramics.* 2000;20:1.
68. Feng X, Huang RYM. Permeate pressure build-up in shellside-fed hollow fiber pervaporation membranes. *Canadian Journal of Chemical Engineering*. 1995;73:833-843.

Manuscript received Oct. 21, 2003, and revision received Apr. 30, 2004.